NASA Technical Memorandum 109009 NASA-TM-109009 19940008377

A Method of Predicting Quasi-Steady Aerodynamics for Flutter Analysis of High Speed Vehicles Using Steady CFD Calculations

Robert C. Scott and Anthony S. Pototzky

July 1993

National Aeronautics and
Space Administration

Langley Research Center
Hampton, Virginia 23681-0001

A METHOD OF PREDICTING QUASI-STEADY AERODYNAMICS FOR FLUTTER ANALYSIS OF HIGH SPEED VEHICLES USING STEADY CFD CALCULATIONS

Robert C. Scott♠
NASA Langley Research Center
Hampton, Virginia

and

Anthony S. Pototzky♣
Lockheed Engineering and Sciences Company
Hampton, Virginia

Abstract

High speed linear aerodynamic theories like piston theory and Newtonian impact theory are relatively inexpensive to use for flutter analysis. These theories have limited areas of applicability depending on the configuration and the flow conditions. In addition, these theories lack the ability to capture viscous, shock and real gas effects. CFD methods can model all of these effects accurately, but the unsteady calculations required for flutter are expensive and often impractical. This paper describes a method for using steady CFD calculations to approximate the generalized aerodynamic forces for a flutter analysis. Example two-and three-dimensional aerodynamic force calculations are provided. In addition, a flutter analysis of a NASP-type wing will be discussed.

Nomenclature

A_0 = real part of GAF
A_1 = imaginary part of GAF
AIC = aerodynamic influence matrix
b = wing semichord
Cp = pressure coefficient, $(p\text{-}p_\infty) / \overline{q}$
d = arbitrary scale factor, $\hat{q}_j/V_\infty$
GAF = generalized aerodynamic force matrix
k = reduced frequency, $\omega b/V_\infty$
p = pressure
q_j = j^{th} generalized coordinate
$\hat{q}_j$ = arbitrary scale factor used in calculation of real pressures for j^{th} mode
$\hat{q}_j$ = arbitrary scale factor used in calculation of imaginary pressures for j^{th} mode
$\overline{q}$ = dynamic pressure, $1/2\rho_\infty V_\infty^2$
S = surface grid contour
S_o = initial surface grid contour
$\hat{S}_j$ = surface grid contour deformed into j^{th} mode shape
t = time
V = velocity
w = normal wash
Ws = steady state mass flux vector
x = x-coordinate
y = y-coordinate
Z = vertical deformation of surface
$z_{0,j}$ = complex amplitude of jth mode
z = z-coordinate
ϕ_j = j^{th} mode shape function
$\hat{\phi}_j$ = j^{th} integrated mode shape function for calculating imaginary pressures
ρ = density
ω = circular frequency

Superscripts/Subscripts

R = real part of quantity
I = imaginary part of quantity
ss = steady state or static aeroelastic value of quantity
∞ = free stream value of quantity

Introduction

The NASP vehicle in its ascent trajectory will be required to fly through an extraordinary range of Mach number conditions. Presently, reliable and accurate linear lifting surface theory codes exist for predicting unsteady aerodynamic forces and performing flutter analyses for general configurations at subsonic Mach numbers and low supersonic Mach numbers. For Mach numbers above 3.0, methods such as piston theory[1] and Newtonian impact theory[2] have been used to predict the unsteady aerodynamic forces. However at the higher Mach numbers, the validity of using these quasi-steady methods becomes more questionable.

Piston theory and Newtonian impact theory are both based on the assumption that the flow is a point function, that is, the pressures are only dependent upon the local conditions. The validity in using these methods is an issue involving both the speed range and the complexity of the vehicle geometry. For piston theory to be valid, it is necessary to have a narrow flow region between the aerodynamic surface and the shock imparted by the surface's leading edge. However, the locations of these regions can change as a result of changes in speed or vehicle angle of attack. In any case, if the flow is such that the shock envelops the aerodynamic surface, then Newtonian impact theory could be used. An aspect of the aerodynamics that is totally disregarded by both of these theories is the interaction between, and the edge effects of, the various aerodynamic surfaces. Also not modeled are viscous, real gas and ionization effects that may occur at very high Mach numbers.

Generally, piston and Newtonian impact theories can not account for the many unknowns at hypersonic conditions and should be used only when "approximate" aerodynamics are acceptable, such as, during the preliminary stages of aircraft design or analysis. The best way to determine the accuracy and region of applicability of these simple methods is by comparing the aerodynamic force predictions with results from more exact aerodynamic theories, such as, Euler or Navier-Stokes theories. The quasi-steady theory, described next, is being developed to provide accurate predictions of aeroelastic response for those flight conditions where the assumptions defined by these simple methods are violated.

Unsteady CFD calculations may be used for flutter calculations and provide improved accuracy over piston and impact theories. The unsteady CFD calculations required to determine a flutter point are computationally expensive. Steady CFD solutions, on the other hand, are easier to obtain. This paper describes the development of a quasi-steady approach for

♠ Aerospace Engineer, Member AIAA.
♣ Staff Engineer, Senior Member AIAA.

using steady CFD calculations to estimate the unsteady aerodynamic forces necessary for flutter calculations. The approach uses two separate CFD solutions per vibratory mode: one solution for the real part of the pressures and another for the imaginary part of the pressures. These pressures are then used to calculate the generalized aerodynamic force (GAF) matrices that can be used in a conventional frequency domain flutter analysis.

This paper is subdivided into three main sections. The first section describes the concept of quasi-steady aerodynamics. It is designed to acquaint the unfamiliar reader with basic concepts that will be built upon in the development of the quasi-steady CFD method. The second section describes the method and presents example two- and three-dimensional aerodynamic calculations. The third section discusses flutter analyses of a high-speed wing at several Mach numbers. The example quasi-steady CFD calculations will be compared with unsteady CFD calculations were available, and all the results will be compared with piston theory results.

Quasi-Steady Concept

The quasi-steady concept as applied to complex hypersonic flow conditions takes advantage of small perturbations and the small time-constants of high velocity flow. In applying the small perturbations to the flow, it is assumed that the complex flow phenomena described by the Euler or Navier-Stokes theory varies linearly if the vehicular motions induced into the flow are considered small enough. With small perturbations, various concepts of frequency domain and superposition can be applied directly to CFD results as it has been employed in piston theory and linear potential theory.

The objective of this work is to incorporate these concepts to the steady pressure distributions and resulting aerodynamic forces predicted by Euler or Navier-Stokes theories so that conventional frequency domain flutter analysis approaches can be applied. This approach, which assumes the flow conditions change almost instantaneously when perturbed, takes advantage of the quasi-steady aspect of the flow physics at high Mach number conditions and can be explained in terms of the reduced frequency, $k = b\omega/V_\infty$.

The reduced frequency characterizes the unsteadiness of the flow. As the velocity of the flow becomes very large, the reduced frequency at flutter will eventually fall within the quasi-steady range ($k<<1$). Also at high Mach numbers, the flow characteristics become dependent more on local conditions. Thus, for decreasing k or increasing Mach number, the flow characteristics approach a point relationship where pressures are dictated only by the flow tangency condition at that point.

For the quasi-steady approach, the flow tangency boundary condition is the primary source of the flow unsteadiness at high Mach numbers. As described in Equation (1), the quasi-steady pressure distribution is obtained by multiplying the aerodynamic influence coefficient (AIC) matrix at zero reduced frequency by the unsteady normalwash vector w.

$$\Delta p(x,y) = AIC_{(k=0)}\, w(x,y,t) \qquad (1)$$

The unsteady normalwash, which defines the kinematic boundary conditions, is given by

$$w(x,y,t) = \partial Z/\partial x + (1/V_\infty)\, \partial Z/\partial t \qquad (2)$$

For harmonic motion, the vertical deformation of the surface is describe by

$$Z(x,y,t) = \sum_{j=1}^{n} \phi_j(x,y) Z_{0,j} e^{i\omega t} = \sum_{j=1}^{n} \phi_j(x,y) q_j \qquad (3)$$

The normalwash boundary condition shown in equation (4) is used in an aerodynamic calculation to obtain the pressure differential for the jth mode (Δp_j).

$$w_j(x,y) = \partial\phi_j / \partial x + i(k/b)\phi_j \qquad (4)$$

The elements of the quasi-steady generalized aerodynamic force (GAF) matrix are defined by

$$GAF_{ij} = \iint_{Area} \Delta p_j(x,y)\phi_i(x,y)dxdy \qquad (5)$$

where i represents the displacement mode (ith rigid or elastic mode deformation) and j represents the pressure mode (pressure distribution resulting from jth rigid or elastic mode deformation).

For quasi-steady flow, the elements of the GAF matrix can be described as linear functions of reduced frequency and have the form,

$$GAF(i\omega)_{ij} = A_{0ij} + i\,(k/b)\, A_{1ij} \qquad (6)$$

where A_0 and A_1 are real matrices. With the GAF matrices accurately represented by linear functions of the reduced frequency, as in equation (6), the aeroelastic equations of motion in state-space form can be developed. The next section describes how these matrices will be obtained from steady CFD calculations.

Description of Quasi-Steady Method

The approach described in this section uses the concepts of three-dimensional flow for both the boundary conditions and the generalized force relationships. As mentioned previously, the method requires that the flow be perturbed by the aerodynamic surfaces only by small amounts so that the superposition principle can be applied. Also, the method relies on the separation of the boundary condition into a steady or real part and a motion or imaginary part. A solution of each part of the boundary conditions constitutes a separate steady CFD solution.

The first subsection presents a description of the boundary conditions imposed for the quasi-steady CFD method. The second and third subsections discuss example two- and three-dimensional calculations, respectively. The CFD flow solver used was CFL3D[3] which can perform either Euler or Navier-Stokes calculations on two- and three-dimensional grids.

Application of Quasi-Steady Boundary Conditions

The CFD quasi-steady method requires only steady CFD solutions in which special boundary conditions are used to provide the appropriate pressure distributions for calculating the GAF matrices. To obtain the individual parts of the GAF matrices, two steady state pressure mode solutions are required per vibratory mode. One solution provides the real part of the pressure, while the other solution provides the imaginary part of the pressure. Only one method is discussed for obtaining the real part; however, two methods are proposed for the imaginary part.

The CFD quasi-steady method is a perturbation approach in which motion is assumed to be small and centered about the static aeroelastic solution. A symmetric aeroelastic vehicle flying at zero angle of attack will experience zero pressure differential and its static aeroelastic shape will retain its undeformed shape, S_o. In general, however, aeroelastic vehicles are asymmetric and fly at non zero angles of attack. The resulting static aeroelastic solution results in non zero steady state pressures and structural deflections.

Assuming only vertical modal deformation, the general aeroelastic vehicle shape is

$$S(x,y,z,t) = Z(x,y,t) + S_{ss}(x,y,z) \tag{7}$$

where S_{ss} is the static aeroelastic shape of the surface grid. Since flutter calculations require only the pressures due to the perturbation motion about S_{ss}, the pressure differentials for the static aeroelastic solution ($\Delta C_{p\,ss}$) must be removed from the unsteady pressures prior the calculating the GAF matrices.

Real Part. To calculate the real part of the pressures the grid geometry for the static aeroelastic shape is deformed to incorporate mode shape deflections. The boundary condition imposed by additively deforming the steady state surface grid geometry into the j[th] mode shape is

$$\hat{S}_j(x,y,z) = \phi_j(x,y)\hat{q}_j + S_{ss}(x,y,z) \tag{8}$$

Where $\hat{q}_j$ is the value of the modal scale factor used to scale the mode shape deformation by an arbitrarily small amount, ϕ_j is the mode shape function, and $\hat{s}$ is a function that describes the contour of the deflected structure.

Using the deformed grid ($\hat{s}$) the pressures for a given Mach number are calculated using the CFD code. These pressures are then used to calculate the real part of the pressure differential for the j[th] mode, where

$$\Delta Cp_j^R(x,y) = (Cp_{upper}(x,y,\hat{q}_j) - Cp_{lower}(x,y,\hat{q}_j)) - \Delta C_{p\,ss} \tag{9}$$

After calculating ΔCp_j^R for all the modes, the A_0 matrix can be calculated from

$$A_{0ij} = \frac{1}{\hat{q}_j} \iint_{Area} \Delta Cp_j^R(x,y)\phi_i dxdy \tag{10}$$

Note that the scale factor value ($\hat{q}_j$) is included in equation (10) so that the product of ΔCp_j^R and $1/\hat{q}_j$ provides the delta pressure per unit generalized coordinate for the j[th] mode.

Imaginary Part. Two methods of providing the boundary conditions necessary for calculating the imaginary part of the GAF matrices are considered. One method is similar to the method described for the real part where the grid is deformed to provide the boundary condition. The other method uses the static aeroelastic grid, S_{ss}, but requires that a transpiration velocity be applied to the surface of the body. Both of these approaches are presented here.

Integration Method. The imaginary part of the pressure is generated by the motion of the wing itself. Generally, most steady CFD codes require the flow tangency condition as the boundary condition quantified by

$$W_s \cdot \nabla S = 0 \tag{11}$$

where W_s is the steady state mass flux vector and ∇S is the surface gradient representing a surface normal. Because this relationship is "built into" most CFD codes, to represent the flow tangency boundary condition it is necessary to appropriately modify the mode shape deflections to simulate the imaginary part of the boundary condition.

Equation (2) provides the appropriate relationship for modifying the mode shapes. To obtain a grid shape that provides the same boundary condition as the vehicle motion, the downwash is set to zero as described in reference 4. By substituting the contribution from the j[th] mode for Z, the relationship becomes

$$\frac{\partial \phi_j}{\partial x} = \frac{-1}{V_\infty}\phi_j\dot{q}_j \tag{12}$$

By redefining the generalized coordinate as the modal scale factor $\hat{q}_j$ and redefining the left hand mode shape function as $\hat{\phi}$, equation (12) becomes

$$\frac{\partial \hat{\phi}_j}{\partial x} = \frac{-1}{V_\infty}\phi_j(x,y)\hat{q}_j \tag{13}$$

Integrating in the x-direction gives the equivalent deformed shape. For a wing this method is implemented by integrating from the leading edge to the trailing edge for each spanwise station

$$\hat{\phi}_j(x,y) = \frac{-\hat{q}_j}{V_\infty}\int_{x=x_{le}}^{x=x_{te}} \phi_j(x,y)dx \tag{14}$$

The surface computational grid is then deformed by the integrated mode shape as

$$\hat{S}_j(x,y,z) = S_{ss}(x,y,z) + \hat{\phi}_j(x,y) \tag{15}$$

Using the grid defined by $\hat{S}_j$ and the CFD flow solver, the pressure differential between the upper and lower surfaces is

$$\Delta C^I{}_{pj}(x,y) = (C_{pupper}(x,y,\hat{q}_j) - C_{plower}(x,y,\hat{q}_j)) - \Delta C_{p\,ss} \tag{16}$$

and the term A_{1ij} is

$$A_{1ij} = \frac{V_\infty}{\hat{q}_j} \iint_{Area} \Delta Cp_j^I(x,y)\phi_i dxdy \tag{17}$$

It is convenient to define

$$d = \frac{\hat{q}_j}{V_\infty} \tag{18}$$

which results in the following,

$$\hat{\phi}_j(x,y) = -d\int_{x=x_{le}}^{x=x_{te}} \phi_j(x,y)dx \tag{19}$$

$$A_{1ij} = \frac{1}{d} \iint_{Area} \Delta Cp_j^I(x,y)\phi_i dxdy \tag{20}$$

Transpiration Method. The transpiration boundary condition method is another approach for calculating the imaginary part of the pressures. Again, the method is only applicable to small perturbation theory conditions. A benefit of this method is that the surface grid does not need to be deformed into the integrated mode shapes. The procedure of deforming the grid can be very time consuming especially for complicated configurations. In the present implementation of the method, the transpiration boundary condition is added to the other boundary conditions as input to the CFD code. The downwash velocity on the surface of the body becomes

$$w_j(x,y) = \frac{\hat{q}_j}{V_\infty}\phi_j(x,y) \tag{21}$$

The pressure differential between the upper and lower surface less the steady state pressure differential is

$$\Delta C^I{}_{p_j}(x,y) = (C_{p_{upper}}(x,y,\hat{q}_j) - C_{p_{lower}}(x,y,\hat{q}_j)) - \Delta C_{p\,ss} \quad (22)$$

Using the $\Delta C_{p_j}{}^I$ and d from equation (18), the downwash velocity and the imaginary part of the GAF matrices are computed as

$$w_j(x,y) = d\,\phi_j(x,y) \quad (23)$$

$$A_{Iij} = \frac{1}{d}\iint_{Area} \Delta C_p{}^I{}_j(x,y)\phi_i dxdy \quad (24)$$

Example Calculations in Two Dimensions

This subsection provides example quasi-steady calculations of the real and imaginary parts of the aerodynamic forces for a two-dimensional airfoil using the quasi-steady CFD (QSCFD) method. Two alternative methods of computing these forces are shown for comparison. One method is to perform unsteady CFD calculations at a low reduced frequency to obtain the aerodynamic forces. The other method is to calculate the aerodynamic forces using piston theory. The mode shape considered was rigid pitching of an airfoil about its leading edge.

While $\Delta C_{p\,ss}$ is in general non zero, the examples discussed in this paper are symmetrical airfoil sections at zero angle of attack. Consequently, the steady state shape is equal to the undeformed shape S_o, and the steady state pressure $\Delta C_{p\,ss}$ is zero.

The 153x41 computational grid used in the two-dimensional CFD calculations is shown in figure 1. The airfoil section is 4% thick and representative of current NASP designs. This grid was used directly for the unsteady CFD calculations and deformed as necessary for the QSCFD calculations.

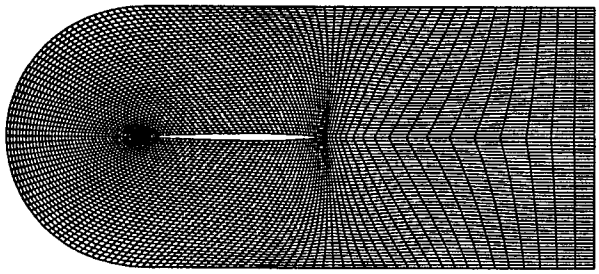

Fig. 1. 153X41 grid for two-dimensional calculations.

The QSCFD method was performed for Mach numbers of 5, 10 and 15. For the real part, the airfoil was deformed into the pitching mode shape. Since the mode shape is rigid pitching, the calculations need only be performed with the grid at an angle of attack. The calculations were performed with an angle of attack of 1 degree with respect to the far field flow. This 1 degree deflection was considered to fall within the limits of small perturbation theory.

Both the integration and transpiration quasi-steady approaches were used to calculate the imaginary part of the lift coefficient. For the calculation of the imaginary part using the integration approach, the grid was deformed into the shape shown in figure 2. For the calculation of the imaginary part with the transpiration approach, a velocity boundary condition was applied to the airfoil surface that was proportional to the mode shape as defined by equation (23).

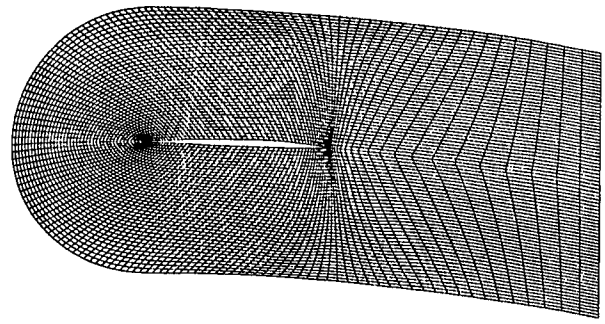

Fig. 2. 153X41 grid for calculating the imaginary part of the lift coefficient.

Unsteady calculations were performed for the airfoil pitching about its leading edge with a reduced frequency of 0.1012 for Mach numbers 5 and 10. At Mach 15, extremely small time steps were required to maintain stability and the unsteady answers were not obtained. The real and imaginary parts of the lift coefficient can be obtained by assuming that the pressures take the form of equation (6) and that there are no higher harmonics. Thus, the real part of the pressure distribution is obtained at a point in the pressure time history where maximum pitch angle and zero angular rate occurs. Similarly, the imaginary part of the pressure distribution is obtained at the point where pitch angle is zero and angular rate is maximum.

Tables 1 and 2 contain results for the real and imaginary parts of the lift coefficient, respectively. At Mach 5 both the real and imaginary parts for all the methods were in good agreement. At Mach 10 the unsteady and quasi-steady answers remain in good agreement, while the piston theory answer begins to differ. At Mach 15 the piston theory and quasi-steady answers are significantly different as expected.

The imaginary calculations using the two QSCFD approaches are compared in table 2. The two methods are in close agreement at all Mach numbers examined. While both methods produce nearly the same results, the transpiration approach is simpler to implement and will be the preferred approach throughout the paper.

Table 1. Real part of the lift coefficient.

Mach	Unsteady CFD (k=0.1012)	Piston Theory	QSCFD (α=1°)
5	0.01457	0.0139	0.0146
10	0.00773	0.00696	0.0081
15	NA	0.00463	0.0057

Table 2. Imaginary part of the lift coefficient.

Mach	Unsteady CFD (k=0.1012)	Piston Theory	QSCFD Integration	QSCFD Transpiration
5	0.00263	0.00268	0.00297	0.00282
10	0.00651	0.000545	0.000687	0.000675
15	NA	0.0001766	0.000294	0.000299

Example Calculation in Three Dimensions

This sub section describes example calculations for a finite wing. Here, unsteady results will be compared with QSCFD results. The mode shape examined was rigid wing pitching about the 65% root chord point. The configuration examined was a generic hypersonic wing having the same airfoil shape as shown in figure 1 and the planform shown in figure 3. The grid used in the calculations was the 153X41X37 C-H grid shown figure 4. CFL3D was the CFD code employed.

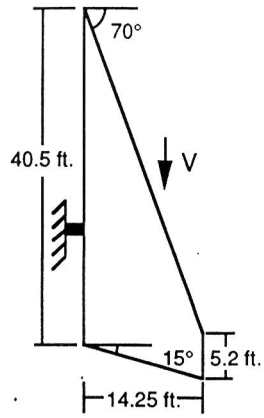

Fig. 3. Wing planform.

The unsteady calculation was performed at a reduced frequency of 0.0506 and the magnitude of pitching oscillation was ±1 degree. Two pressure distributions were extracted from the time history of the unsteady calculation as described in the previous subsection. The real and imaginary pressure distributions using the quasi-steady and unsteady calculations are shown in figures 5 and 6, respectively. Good agreement was achieved for both the real and imaginary parts of the pressures.

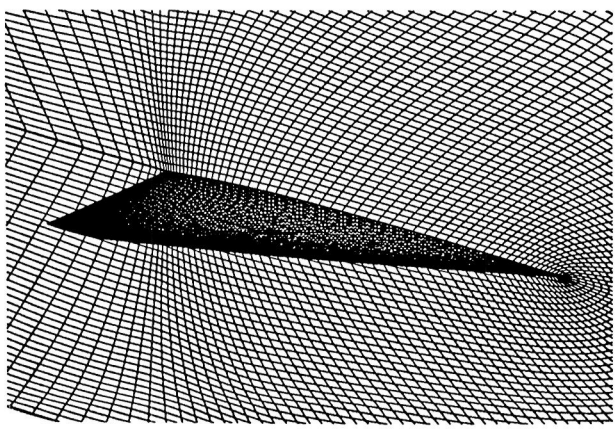

Fig. 4. 153X41X37 C-H grid for the wing.

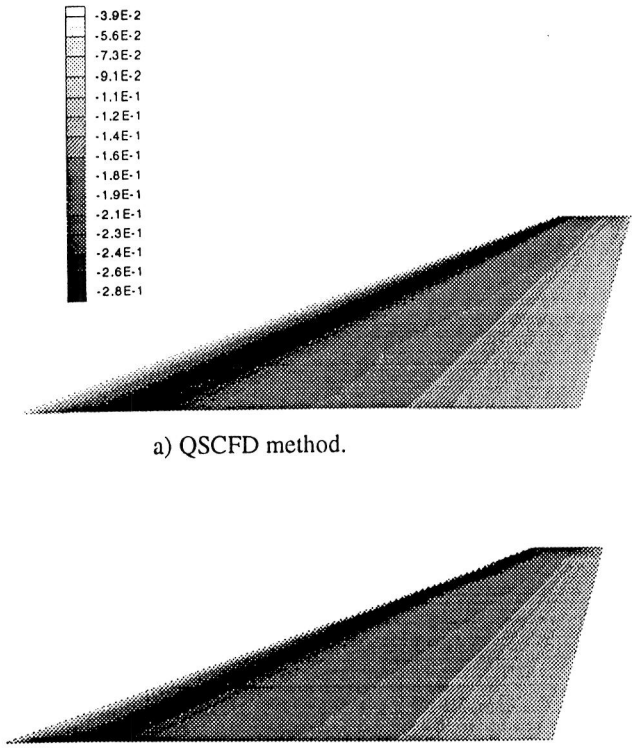

a) QSCFD method.

b) Unsteady CFD method, k=0.0506.

Fig. 5. Comparison of real pressure coefficient distribution computed with QSCFD and unsteady CFD methods.

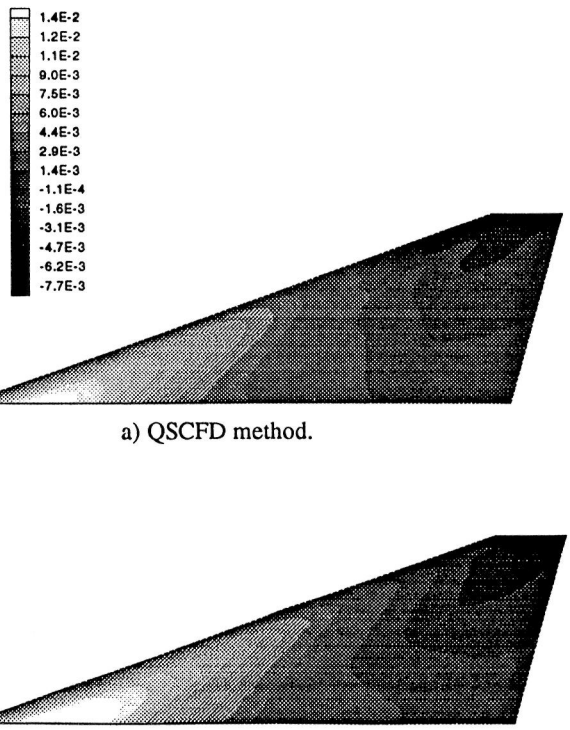

a) QSCFD method.

b) Unsteady CFD method, k=0.0506.

Fig. 6. Comparison of imaginary pressure coefficient distribution computed with QSCFD and unsteady CFD methods.

Flutter Analysis

This section of the paper describes flutter calculations for a hypersonic wing having eight flexible modes using the QSCFD method. The planform and computational grid for the wing are shown in figures 3 and 4, respectively.

Calculations were performed at Mach numbers of 5, 10 and 15. Three results were obtained at each Mach number. Two of the results were obtained using the QSCFD method to calculate the unsteady pressures; one with and the other without the spanwise flux terms included. Neither unsteady CFD flutter results nor experimental results were available for this configuration. Piston theory results are provided for comparison.

QSCFD GAF Calculations

The subsection describes the QSCFD calculations of the unsteady pressures and GAF matrices. Comparisons of the real and imaginary parts of the pressure coefficients for flexible mode 4 at Mach 5 are also provided. Mode 4 was selected because it will be shown in the next subsection to be the dominant component of the flutter mode at Mach numbers of 5 and 10.

As mentioned earlier, two sets of QSCFD calculations were performed. One is referred to as the QSCFD 2d results because the spanwise flux terms were zero. The other is referred to as the QSCFD 3d results because the spanwise flux terms were included.

To calculate the real part of the pressure, the undeformed grid shown in figure 4 was used as a starting point and separate grids were generated by deforming that grid into shapes corresponding to each of the eight wing mode shapes. Figure 7 shows the deflection contour for the 4th flexible mode. Each of these eight grids was used to obtain the wing surface pressure distribution per unit deformation for each mode and Mach number combination. Using these pressure distributions and the wing mode shapes, the real parts of the GAF matrices were then calculated. These values constitute the elements of A_0 in equation (6).

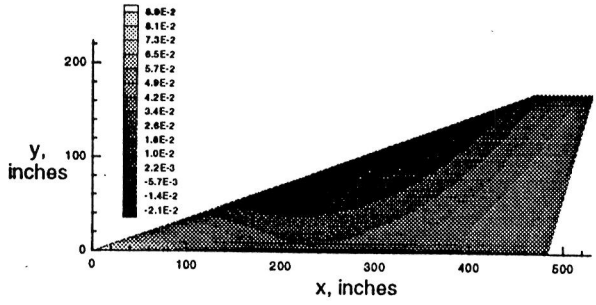

Fig. 7. Deflection contour for the 4th flexible mode.

To calculate the imaginary parts of the pressure, a data file was created for each mode that contained the desired vertical velocity on the surface of the wing. By performing separate steady-state calculations for each mode shape data file and Mach number combination, the imaginary parts of the pressures were calculated. These pressure distributions and the mode shapes were then used to calculate the imaginary parts of the GAF matrices represented by A_1 in equation (6).

Figures 8 and 9 compare the Mach 5 real and imaginary pressures, respectively, associated with the 4th mode. Figure 8 indicates good agreement among the three results for the real part of the pressures. Figure 9 indicates good agreement between the imaginary pressures from the QSCFD 2d calculations and the piston theory calculations. While similar in character, the QSCFD 3d imaginary results are somewhat different from the others.

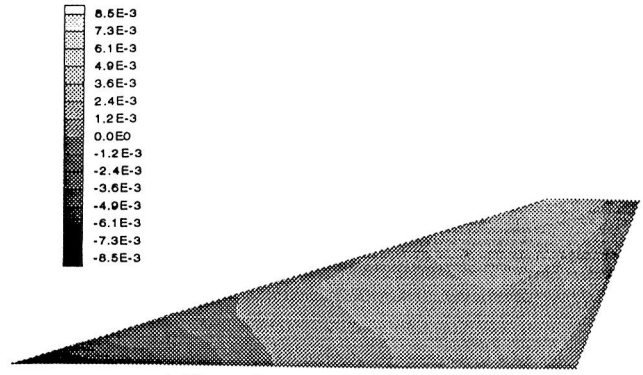

a) Piston theory calculation.

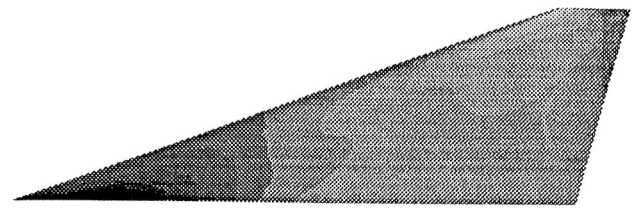

b) QSCFD 2d calculation.

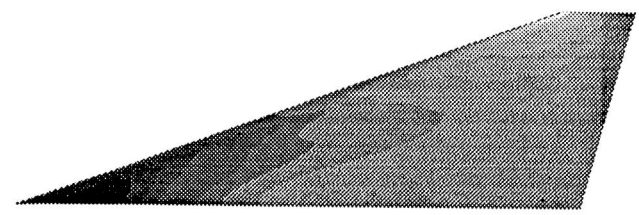

c) QSCFD 3d calculation.

Fig. 8. Real part of Mach 5 pressure coefficient contours associated with mode 4.

Two distinct trends were observed in the pressure contour plots as Mach number was increased from 5 to 15. First, the QSCFD 2d and 3d pressure distributions became increasingly similar. Second, the piston theory pressure distributions became significantly different from the QSCFD pressures. The effects of these trends subsequently showed up in the flutter analysis results described in the next subsection.

Flutter Calculation

A comparison of the flutter root locus was undertaken for the different aerodynamic analysis methods and Mach numbers. The purpose of the study was to assess the effect of the GAF matrices produced by the aerodynamic methods on flutter. The structural parts, that is, the vibration frequencies, generalized masses, mode shapes, and structural damping, are identical for all cases. The flutter equations of motion were transformed to 1st order form using the ISAC[5] code. This code was used to obtain the A_0 and A_1 aerodynamic matrices as defined by equation (6). Matched point flutter analyses were performed where the altitude range was varied from sea level to 80,000 feet.

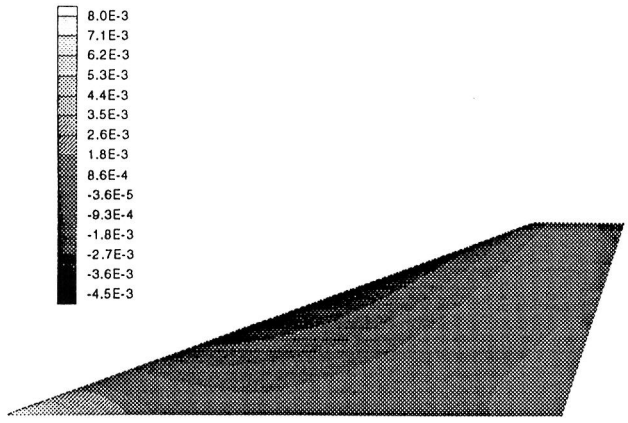

a) Piston theory calculation.

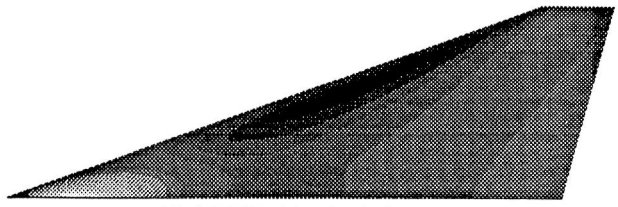

b) QSCFD 2d calculation.

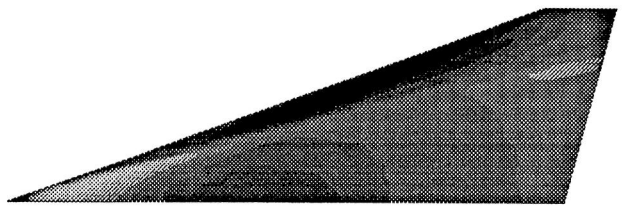

c) QSCFD 3d calculation.

Fig. 9. Imaginary part of Mach 5 pressure coefficient contours associated with mode 4.

The results for all the flutter analyses are summarized in table 3. In all cases the primary mechanism for aeroelastic instability is divergence. The reason for this instability can be attributed to the pivot point being very far aft on the wing as seen in figure 3. In order to compare effects of the various aerodynamic methods on flutter, the dynamic pressure of the first and, where applicable, the second dynamic instability points are shown.

Figure 10 shows the root locus results for the three aerodynamic calculations at Mach 5. The root locus plots generally look very similar for all the aerodynamic methods, and a hump mode is the cause of the flutter instability for both the QSCFD 2d and piston theory results at Mach 5. Much the same type of behavior is noted for this mode in the QSCFD 3d results. However, the inclusion of the spanwise flux terms into the CFL3D calculations has altered the pressures enough to move the hump mode into a stable region as illustrated in figure 10(c).

Except for the Mach 5 result, the QSCFD 2d and 3d results are in good agreement for all the quantities provided in table 3. Piston theory is shown to increasingly under-predict flutter and divergence dynamic pressure as compared with the QSCFD calculations as Mach number increases.

The piston theory flutter frequency is in good agreement with the QSCFD 2d frequency at Mach 5 indicating similar flutter mechanisms. At Mach 10 the frequencies of the first and second instability are consistent indicating similar flutter mechanisms for both the QSCFD and piston theory calculations. At Mach 15 the piston and QSCFD calculations each predict different primary flutter mechanisms. This is attributed to the fact that piston theory predicted imaginary GAF elements significantly larger than those predicted by the QSCFD calculations.

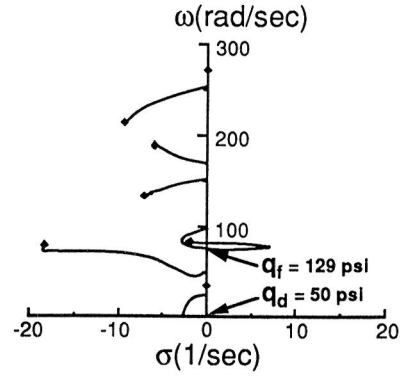

a) Using piston theory GAF matrices.

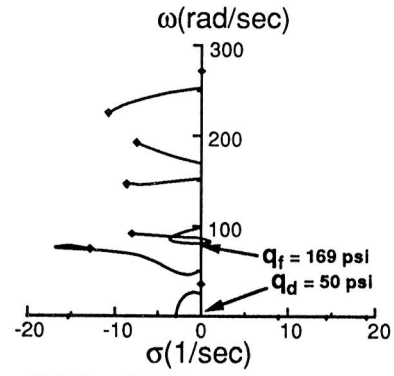

b) Using QSCFD 2d GAF matrices.

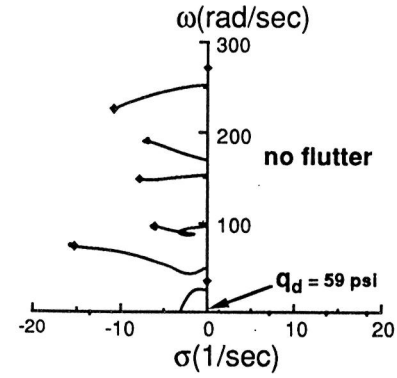

c) Using QSCFD 3d GAF matrices.

Fig. 10. Mach 5 root locus results.

Table 3. Comparison of flutter results.

Aerodynamic methods		Mach number 5			10			15		
		q_f psi	ω_f r/s	q_d psi	q_f psi	ω_f r/s	q_d psi	q_f psi	ω_f r/s	q_d psi
Piston theory	1st	129	78	50	184	78	66	250	72	81
	2nd	-	-	-	537	186	-	634	181	-
QSCFD 2d	1st	169	80	50	331	81	109	982	224	271
	2nd	-	-	-	578	212	-	-	-	-
QSCFD 3s	1st		-	59	330	82	114	981	224	267
	2nd	-	-	-	586	208	-	-	-	-

If the quasi-steady method can be considered the more accurate method for computing the aerodynamic forces, then from both the stand point of the root locus plots and the flutter and divergence dynamic pressures, piston theory shows limited accuracy with large conservatism at elevated Mach numbers.

Recommendations

All the CFD calculations presented in this paper used Euler equations. While solutions of the Euler equations can be obtained over a wide range of flow conditions, viscous effects may be required in certain instances to get accurate solutions. Consequently, future applications of the QSCFD method should consider using solutions of the Navier-Stokes equations when viscous effects are expected to have a significant impact on pressure distributions.

The same grid was used for all the QSCFD calculations used in the flutter analyses. To get CFD solutions of the highest accuracy it is often required that grids be designed with some a priori knowledge of the flow field solution or that the CFD code has adaptive mesh refinement capabilities. Since making computational grids is a time consuming process, the use of such an adaptive code is an ideal way to improve solution accuracy without increasing the analyst's workload.

While the QSCFD pressures have been compared with unsteady pressures for a single mode at a time, the general applicability of the superposition assumption has not been completely answered for flexible modes. In addition, the QSCFD flutter results have only been compared with calculations using piston theory. To fully validate the method, unsteady CFD flutter analysis results need to be compared with a QSCFD flutter analysis.

The selection of the perturbation scale factors was not addressed in the paper. In highly nonlinear flow the linearized aerodynamics from the QSCFD method could be very sensitive to the quantities chosen as scale factors. The sensitivities of these scale factors need to be considered when performing the QSCFD analysis.

Concluding Remarks

Because of the extremely high cost of performing time-accurate unsteady CFD calculations required for a flutter analysis and the lack of other, accurate, computationally efficient means of obtaining the aerodynamics at hypersonic Mach numbers, a new approach requiring only steady CFD computations has been developed. The quasi-steady CFD method uses special boundary conditions for computing the unsteady pressures from steady CFD calculations. These pressures can then be used to calculate the generalized aerodynamic force matrices for use in conventional flutter analyses. The quasi-steady CFD method was demonstrated using two- and three-dimensional calculations at supersonic and hypersonic Mach numbers.

The quasi-steady CFD aerodynamics should be more accurate and potentially less conservative than that obtained by piston and Newton impact theories. More accurate aerodynamics will bring about more realistic flutter sizing and possibly lighter structural weights for hypersonic vehicles. The quasi-steady technique goes beyond piston theory by including the steady nonlinear aerodynamic effects of the perturbation point. Thus, this paper has presented an efficient means of using high fidelity aerodynamics in a relatively computationally efficient flutter analysis.

Acknowledgment

The authors would like to thank Dr. Thomas A. Zeiler of Lockheed Engineering and Sciences Company for providing the structural mode shape data and the piston theory data used in this paper. In addition, the authors would also like to thank Elizabeth Lee-Rausch of NASA Langley's Unsteady Aerodynamics Branch for her assistance in grid generation and using CFL3D.

References

1. Morgan, H.; Huckel, V.; and Runyan, H.: Procedure for Calculating Flutter at High Hypersonic Speed Including Camber Deflection, and Comparison with Experimental Results. NACA TN-4335, September 1958.

2. Yates, E. C.; and Bennett, R. M.: Analysis of Supersonic-Hypersonic Flutter of Lifting Surfaces at Angle of Attack. AIAA Paper No. 71-327, presented at the AIAA 12th Structures, Structural Dynamics and Materials Conference, April 1971.

3. Walters, R.; Reu, T.; McGrory, W.; Thomas, J.; and Richardson, P.: A Longitudinally-Patched Grid Approach with Applications to High Speed Flows. AIAA Paper No. 88-0715, AIAA 26th Aerospace Sciences Meeting, Reno, Nevada, January 1988.

4. Etkin, B. Z: Dynamics of Flight. John Wiley and Sons, New York, NY, 1982.

5. Peele, E. L.; and Adams, W. M.: A Digital Program for Calculating the Interactions Between Flexible Structures, Unsteady Aerodynamics and Active Controls. NASA TM-80040, January 1989.

REPORT DOCUMENTATION PAGE

Form Approved
OMB No. 0704-0188

1. AGENCY USE ONLY (Leave blank)	2. REPORT DATE	3. REPORT TYPE AND DATES COVERED
	July 1993	Technical Memorandum

4. TITLE AND SUBTITLE

A Method of Predicting Quasi-Steady Aerodynamics for Flutter Analysis of High Speed Vehicles Using Steady CFD Calculations

5. FUNDING NUMBERS

WU 505-63-50-15

6. AUTHOR(S)

Robert C. Scott and Anthony S. Pototzky

7. PERFORMING ORGANIZATION NAME(S) AND ADDRESS(ES)

NASA Langley Research Center
Hampton, VA 23681-0001

8. PERFORMING ORGANIZATION REPORT NUMBER

9. SPONSORING / MONITORING AGENCY NAME(S) AND ADDRESS(ES)

National Aeronautics and Space Administration
Washington, DC 20546-0001

10. SPONSORING / MONITORING AGENCY REPORT NUMBER

NASA TM-109009

11. SUPPLEMENTARY NOTES

Presented at the AIAA 34th Structures, Structural Dynamics, and Materials Conference, 4/19-21/93, LaJolla, CA. Scott: NASA Langley Research Center, Hampton, VA.; Pototzky: Lockheed Engineering and Sciences Co., Hampton, VA.

12a. DISTRIBUTION / AVAILABILITY STATEMENT

Unclassified - Unlimited

Subject Category 05

12b. DISTRIBUTION CODE

13. ABSTRACT *(Maximum 200 words)*

High speed linear aerodynamic theories like piston theory and Newtonian impact theory are relatively inexpensive to use for flutter analysis. These theories have limited areas of applicability depending on the configuration and the flow conditions. In addtion, these theories lack the ability to capture viscous, shock and real gas effects. CFD methods can model all of these effects accurately, but the unsteady calculations required for flutter are expensive and often impractical. This paper describes a method for using steady CFD calculations to approximate the generalized aerodynamic forces for a flutter analysis. Example two-and three-dimensional aerodynamic force calculations are provided. In addition, a flutter analysis of a NASP-type wing will be discussed.

14. SUBJECT TERMS

Usteady aerodynamics, quasi-steady aerodynamics, flutter analysis, CFD, structural dynamics

15. NUMBER OF PAGES

10

16. PRICE CODE

A02

17. SECURITY CLASSIFICATION OF REPORT	18. SECURITY CLASSIFICATION OF THIS PAGE	19. SECURITY CLASSIFICATION OF ABSTRACT	20. LIMITATION OF ABSTRACT
Unclassified	Unclassified		